WILEY | Hindawi

Research Article

State of Charge and State of Health Coestimation for Lithium-Ion Capacitor Based on Multi-innovation Filters

Fanqi Min,[1,2,3] **Shiyi Fu,**[3,4] **Wenping Jiang,**[3] **Liheng Zhang,**[1,3,4] **Guoju Dang,**[3,4] **Ying Luo,**[3,4] **Liqin Yan,**[3,4] **Jingying Xie** ORCID,[1,3,4] **Taolin Lv** ORCID,[3,4] **and Yunzhi Gao**[1]

[1]*School of Chemistry and Chemical Engineering, Harbin Institute of Technology, Harbin 150001, China*
[2]*Shanghai Aerospace Power Technology Co., Ltd., Shanghai 201112, China*
[3]*Shanghai Engineering Technology Center of Power and Energy Storage Battery System, Shanghai 200245, China*
[4]*State Key Laboratory of Space Power-Sources Technology, Shanghai Institute of Space Power-Sources, Shanghai 200245, China*

Correspondence should be addressed to Jingying Xie; jyxie@hit.edu.cn and Taolin Lv; a357439607@163.com

The lithium-ion capacitor (LIC) is a new type of hybrid energy storage device, which combines the advantages of lithium-ion battery and electric double layer capacitor. To achieve efficient and reliable application of LIC in practical scenarios, accurate model and state estimation method are needed. In this work, the electrical behavior of LIC is studied, which is then described by the Thevenin model. A multi-innovation filter- (MIF-) based coestimation method is proposed, in which the multi-innovation linear Kalman filter (MI-LKF) is used for model parameter identification, the multi-innovation cubature Kalman filter (MI-CKF) is used for state of charge estimation, and the multi-innovation extended Kalman filter (MI-EKF) is used for state of health estimation. Compared to traditional methods, this method can significantly improve estimation accuracy by only expanding the innovation used to update the state from a single moment to multiple moments. The experimental results indicate that the estimation errors of SOC and SOH can be constrained within ±0.5%. In addition, the proposed method has good robustness and can achieve high-precision state estimation even in the face of noise interference, uncertain initial values of the algorithm, and uncertain starting operating points.

1. Introduction

The whole world is in a critical period of energy transition due to the excessive consumption of fossil fuel and the increasing of environment temperature [1]. In order to achieve the goal of reducing the environment temperature and zero carbon dioxide emissions, countries are trying to increase the penetration of renewable energy and develop green energy storage technology [2, 3]. The lithium-ion capacitor (LIC) is a new type of rechargeable energy storage device, which consists of a lithium-ion battery (LIB) type positive electrode, an electric double layer capacitor (EDLC) type negative electrode, and a Li-ion conducting organic electrolyte [4]. As reported in literatures, the LIC combines the advantages of LIC and EDLC and has the ability to provide high-power density (3-15 kW kg^{-1}) and high-energy density (10-30 Wh kg^{-1}) [5–7].

The LIC has a wide range of application, including stationary energy storage systems and electric vehicles. To ensure the reliability and safety of LIC during its operation, a management system is indispensable, which can monitor the states of LIC in real time and make reasonable operation control strategy [8]. Hence, the accurate modeling and state estimation of LIC have attracted the attention of researchers.

Similar to the LIBs, the internal electrochemical reaction of LIC can be described in detail by an electrochemical

models (EMs), and the external electrical behavior of LIC can be expressed in a simple way by equivalent circuit models (ECMs) and fractional order models (FOMs) [9–11]. In general, modeling with EMs can obtain a very high accuracy. However, plenty of partial differential equations (PDEs) in EMs makes it hard to solve in short time and thus hard to use in practical application. In contrast, the good balance between model complexity and accuracy of ECMs and FOMs has been proven by researchers, and researches aiming at online state estimation have been developed based on these models [12–14].

State of charge (SOC) and state of health (SOH) are two crucial parameters to battery management system (BMS) for LIBs, as they indicate the remaining capacity of current cycle and the ability of long-term cycling of LIBs [15, 16]. The operating mechanism of LIC is similar to LIB; therefore, the estimation of SOC and SOH for LIC is indispensable.

A number of state estimation methods have been put up for LIBs. Among methods for SOC estimation, the simplest one is the ampere hour integration (AHI) method; however, the measurement error and the initial error may make the AHI method failed [17]. The open circuit voltage (OCV) is the most commonly used as the index for the look-up table method as it decreases monotonically with the SOC, but long time rest is needed for obtaining an accurate OCV, which limits its application in online usage scenario [18]. Data-driven method can ignore the physical process and internal reaction of a system; however, it exclusively relies on the quality of dataset and learning method [19]. Compared with the above methods, model-based methods have shown certain advantages and have also received widespread attention. Ref. [20] proposed an improved adaptive square-root cubature Kalman filter (IASRCKF) for LIB SOC estimation, and the impact of parameter settings on its performance was discussed. In Ref. [21], the nonlinear autoregressive exogenous is used to optimize the Levenberg-Marquardt training algorithm, and Bayesian regularization (BR) for LIB SOC estimation, and the author also studied the relationship between the accuracy of NARX technology and the training dataset. In Ref. [4], Yang et al. successfully applied improved cubature Kalman filter (ICKF) to the SOC estimation of LIC, and its effectiveness has been verified under various working conditions, providing a certain reference for the state estimation work of LIC. Compared to the SOC, the SOH is a slow varying parameter. Nevertheless, the online estimate of SOH is significant as it plays a decisive role in the estimation accuracy of SOC. To date, many types of coestimation methods for SOC and SOH of LIBs have been put forward. In [22], Plett achieved real-time estimation of LIB SOH using EKF by reconstructing the SOC equation. In Ref. [23], an adaptive dual square-root Kalman filtering (ADSRCKF) with the dormancy zone is proposed to achieve real-time coestimation for SOC and SOH of LIB.

We found that although there has been in-depth research on the state estimation of LIB and in order to improve the estimation accuracy, existing methods are gradually showing a trend of being more complex, which is unfavorable for
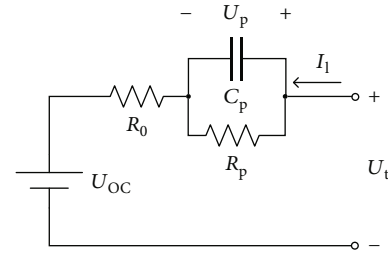

Figure 1: Scheme of the Thevenin model.

future installation on BMS. Meanwhile, to the best of the authors' knowledge, there are few literatures which report the coestimation of LIC SOC and SOH. Hence, this work is aimed at proposing a joint SOC and SOH estimation method suitable for LIC, and this method is as simple and lightweight as possible, with prospects for future deployment in BMS. Main contribution of this work can be summarized as follows: (1) a Thevenin model for LIC is established to simulate its dynamic characteristics. (2) A multi-innovation filter framework is constructed for SOC and SOH estimation of LIC, where the multi-innovation linear Kalman filter (MI-LKF) is used for model parameter identification, the multi-innovation cubature Kalman filter (MI-CKF) is used for SOC estimation, and the multi-innovation extended Kalman filter (MI-EKF) is used for SOH estimation. (3) The robustness of the proposed method was verified under algorithm initial value uncertainty, state actual initial value uncertainty, and noise disturbance.

This work is organized as follows. The modeling of LIC is illustrated in Section 2. The working principles of the proposed MIF-based coestimation method for SOC and SOH are presented in Section 3. The experimental results and analysis are shown in Section 4. Finally, the conclusion is given in Section 5.

2. Modeling of LIC

2.1. Model Selection. Among various types of ECMs, the Thevenin model has been approved to have a good balance between model complexity, accuracy, and generalization for LIBs [24]. The Thevenin model has been proved to be applicable to simulate the voltage response of LIC, and the results show that the Thevenin model can approximately describe the electric behavior of LIC under the conditions of charging, discharging, and shelving [25]. The Thevenin model is shown in Figure 1, which consists of an ideal voltage source, a series resistance, and a RC network. The ideal voltage source U_{OC} represents the OCV of the LIC, which has a functional relationship with the SOC. The series resistance (i.e., ohmic resistance) R_0 is used to characterize the transient response during charge and discharge stages. The polarization resistance R_p and polarization capacitance C_p are connected in parallel to form the RC network, which characterize the polarization effect during charge and discharge stages.
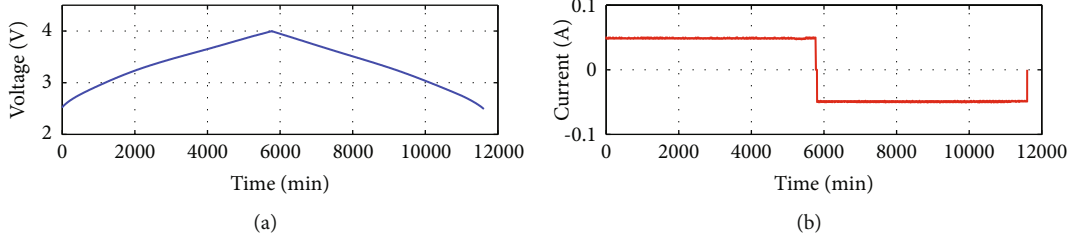
Figure 2: Results of LO test: (a) voltage profile; (b) current profile.

Based on the Thevenin model and the Kirchhoff's law, the electric behavior of LIC can be expressed as follows:

$$
\begin{cases}
U_t = U_{OC} + I_1 R_0 + U_p, \\
I_1 = \dfrac{U_p}{R_p} + C_p \dfrac{dU_p}{dt},
\end{cases}
\tag{1}
$$

where U_t represents the terminal voltage of LIC, I_t represents the load current, and U_p is the polarization voltage. Generally, in order to simulate the behavior of the LIC, Eq. (1) should be expressed in discrete time form, as shown in

$$
\begin{cases}
U_{p,k} = U_{p,k-1} \exp\left(-\dfrac{\Delta t}{R_p C_p}\right) + I_{1,k} R_0 \left(1 - \exp\left(-\dfrac{\Delta t}{R_p C_p}\right)\right), \\
U_{t,k} = U_{OC,k} + U_{p,k} + I_{1,k} R_0,
\end{cases}
\tag{2}
$$

where Δt represents the sampling time and the subscript k represents the kth step.

2.2. OCV Curve Fitting. Low current OCV (LO) test is carried out to obtain the OCV data. Constant current charging of LIC is first carried out with a rate of 0.01 C (approximately 0.05 A) to its upper cut-off voltage. After a shelving time of 30 min, the LIC is then discharged under a constant current with a rate of 0.01 C to its lower cut-off voltage. The results of LO test are shown in Figure 2.

To evaluate the impacts of OCV on the simulation of LIC states, results of the charging process, discharging process, and average of charging and discharging process are taken into account. It should be noted that the average one is calculated according to the following equation:

$$
U_{OC,ave} = \frac{U_{OC,dis} + U_{OC,cha}}{2},
\tag{3}
$$

where $U_{OC,cha}$ represents the OCV obtained from charging LO process, $U_{OC,dis}$ represents the OCV obtained from discharging LO process, $U_{OC,ave}$ represents the average value
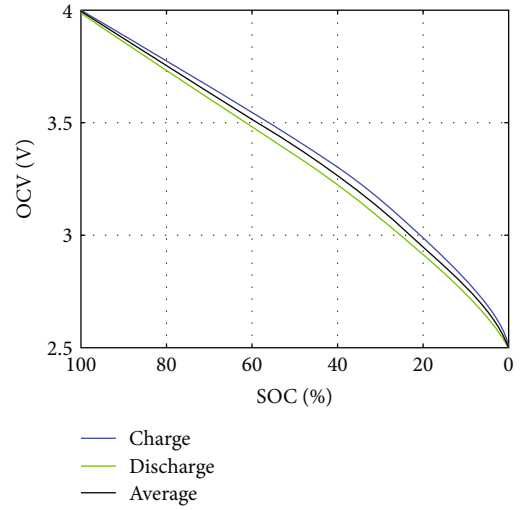

Figure 3: Results of OCV obtained from different LO tests.

of the former two OCV, and these three OCV are shown in Figure 3.

Finally, a polynomial of degree 8 is used to fit the functional relationship between OCV and SOC, which is expressed as

$$
U_{OC} = a_0 + a_1 x + a_2 x^2 + \cdots + a_8 x^8,
\tag{4}
$$

where x represents SOC and $a_i (i = 1, 2, \cdots, 8)$ represents the coefficients need to be fitted.

2.3. MI-LKF-Based Parameter Identification. Besides the OCV curve, the parameters of the electrical components used in the Thevenin model are essential as well. In order to identify the parameters in real time, the relationship between parameters and measurable signals should be expressed in linear form. By applying the bilinear transform to the transfer function, the recursive form of Eq. (1) in discrete time can be obtained. The calculation processes are shown as follows:

$$
\frac{U_t(s) - U_{OC}(s)}{I_1(s)} = \frac{R_0 + R_p + R_0 \tau s}{1 + \tau s},
\tag{5}
$$

Regression model:

$U_{t,k} = \theta_k^{\mathrm{T}} \varphi_k$

Step I: initialization

For $k = 0$, set θ_0, $P_{1,0}$, Q_l, and R_l.

Step II: computation

State prior estimation

$\theta_k^- = \theta_{k-1}$

Error covariance prior estimation

$P_{1,k}^- = P_{1,k-1} + Q_l$

Kalman gain calculation

$K_{1,k} = P_{1,k}^- \varphi_k^T (\varphi_k P_{1,k}^- \varphi_k^T)^{-1}$

Innovation value calculation

$e_{1,k} = U_{t,k} - \theta_k^{-,T} \varphi_k$

Innovation vector and gain vector calculation

$E_{1,L} = [e_{1,k} \quad e_{1,k-1} \quad e_{1,k-2} \quad \cdots \quad e_{1,k-L+1}]^T$

$K_{1,L} = [K_{1,k} \quad K_{1,k-1} \quad K_{1,k-2} \quad \cdots \quad K_{1,k-L+1}]^T$

State posterior estimation

$\theta_k = \theta_k^- + K_{1,L} E_{1,L}$

Error covariance posterior estimation

$P_{1,k} = (I - K_{1,k}\varphi_k) P_{1,k}^-$

where $\theta_k = [a_{0,k} \quad (1 - a_{0,k})U_{OC,k} \quad a_{1,k} \quad a_{2,k}]^T$ represents the identified vector, $\varphi_k = [U_{t,k-1} \quad 1 \quad I_{1,k} \quad I_{1,k-1}]$ represents the input vector, K_1 is the Kalman gain vector of MILKF, P_1 is the covariance matrix, Q_l is the process noise covariance matrix, R_l is measurement noise covariance matrix, and I is the unit matrix.

ALGORITHM 1: Recursive process of MI-LKF.

$$s = \frac{2}{\Delta t} \frac{1 - z^{-1}}{1 + z^{-1}}, \tag{6}$$

$$U_{t,k} = a_0 U_{t,k-1} + (1 - a_0) U_{OC,k} + a_1 I_{1,k} + a_2 I_{1,k-1}, \tag{7}$$

where $\tau = R_p \times C_p$ is the time constant of the RC network. In addition, a_0, a_1, and a_2 are related to R_0, R_p, and τ, and they are expressed as

$$\begin{cases} a_0 = \dfrac{2\tau - \Delta t}{2\tau + \Delta t}, \\[2mm] a_1 = \dfrac{R_p \Delta t + R_0(2\tau + \Delta t)}{2\tau + \Delta t}, \\[2mm] a_2 = \dfrac{R_p \Delta t + R_0(-2\tau + \Delta t)}{2\tau + \Delta t}. \end{cases} \tag{8}$$

With Eq. (6) and Eq. (7), the model parameters can be identified by recursive algorithm, and the applicability of the liner KF (LKF) algorithm in this usage scenario has been proven in our previous work [26, 27]. Nevertheless, the classical filter only uses single innovation to update the estimated states, and more innovations from the model are not utilized. The multi-innovation (MI) algorithm proposed by Ding and Chen in 2007 is to address this issue [28]. With the MI algorithm, the innovation scalar will be extended to a vector, which contains more innovation value. The innovation vector is expressed as

$$E_L = [e_k \quad e_{k-1} \quad e_{k-2} \quad \cdots \quad e_{k-L+1}]^T, \tag{9}$$

where E_L represents the innovation vector, L is the length of the innovation vector, and e_k represents the system error at the kth iterative step. Meanwhile, the corresponding gain will be also expanded to form of vector, which is expressed as

$$K_L = [K_k \quad K_{k-1} \quad K_{k-2} \quad \cdots \quad K_{k-L+1}]^T, \tag{10}$$

where K_L represents the gain vector and K_k represents the gain value at k^{th} iterative step. Then, the state estimated by the MI-based filter algorithm should be updated by

$$x_k = x_k^- + K_L E_L, \tag{11}$$

where x_k represents the estimated state and x_k^- represents the priori estimation of the state.

In this work, the MI-LKF algorithm is implemented for parameter identification of LIC, and the recursive process of MI-LKF is given in Algorithm 1.

3. Coestimation

3.1. MI-CKF-Based SOC Estimation.
The SOC is defined as the ratio of remaining capacity at present to its maximum available capacity, which is expressed as follows:

$$\mathrm{SOC} = \frac{C_{\mathrm{cur}}}{C_{\mathrm{max}}} \times 100\%, \tag{12}$$

where C_{cur} represents the remaining capacity at present and C_{max} is the maximum capacity available. The remaining

Nonlinear system:
$$\begin{cases} x_{c,k} = f_c(x_{c,k-1|k-1}, u_k) + w_k \\ z_k = g(x_{c,k|k}, u_k) + v_k \end{cases}$$
Step I: initialization
  For $k = 0$, set $x_{c,0|0}$, $P_{c,0|0}$, Q_c, and R_c.
Step II: computation
  Time update
  Cubature points evaluation
$$x_{i,k-1|k-1} = S_{k-1|k-1}\xi_i + x_{c,k-1|k-1}$$

where $S_{k-1|k-1}$ is calculated by factorizing $P_{c,k-1|k-1}$ according to $P_{c,k-1|k-1} = S_{k-1|k-1}S_{k-1|k-1}^T$, and $\xi = \sqrt{n}\begin{bmatrix} 1 & 0 & -1 & 0 \\ 0 & 1 & 0 & -1 \end{bmatrix}$

  Cubature points propagation
$$x_{i,k-1|k-1}^* = f_c(x_{i,k-1|k-1}, u_k)$$
  State estimation
$$x_{c,k|k-1} = 1/2n\sum_{i=1}^{2n} x_{i,k-1|k-1}^*$$
  Error covariance estimation
$$P_{c,k|k-1} = 1/2n\sum_{i=1}^{2n} x_{i,k-1|k-1}^* x_{i,k-1|k-1}^{*,T} - x_{k|k-1}x_{k|k-1}^T$$
Measurement update
  Factorization and cubature points evaluation
$$P_{c,k|k-1} = S_{k|k-1}S_{k|k-1}^T$$
$$X_{i,k|k-1} = S_{k|k-1}\xi_i + x_{c,k|k-1}$$
  Cubature points propagation
$$Z_{i,k|k-1} = g(X_{i,k|k-1}, u_k)$$
  Measurement estimation:
$$z_{k|k-1} = 1/2n\sum_{i=1}^{2n} Z_{i,k|k-1}$$
  Innovation covariance matrix estimation
$$P_{zz,k|k-1} = 1/2n\sum_{i=1}^{2n} Z_{i,k|k-1}Z_{i,k|k-1}^T - z_{k|k-1}z_{k|k-1}^T + R$$
  Cross-covariance matrix estimation
$$P_{xz,k|k-1} = 1/2n\sum_{i=1}^{2n} X_{i,k|k-1}Z_{i,k|k-1}^T - x_{c,k|k-1}z_{k|k-1}^T$$
  Kalman gain calculation
$$K_{c,k} = P_{xz,k|k-1}/P_{zz,k|k-1}$$
  Innovation value calculation
$$e_{c,k} = U_{t,k} - z_{k|k-1}$$
  Innovation vector and gain vector calculation
$$K_{c,L} = [K_{c,k} \quad K_{c,k-1} \quad K_{c,k-2} \quad \cdots \quad K_{c,k-L+1}]^T$$
  State updating
$$x_{c,k|k} = x_{k|k-1} + K_{c,L}E_{c,L}$$
  Error covariance estimation
$$P_{c,k|k} = P_{c,k|k-1} - K_{c,L}P_{zz,k|k-1}K_{c,L}^T$$
Here, Q_c is the process noise covariance matrix, R_c is the measurement noise covariance matrix, ξ_i is the ith column of ξ, and n denotes the dimension of state vector and $n = 2$.

ALGORITHM 2: Recursive process of MI-CKF.

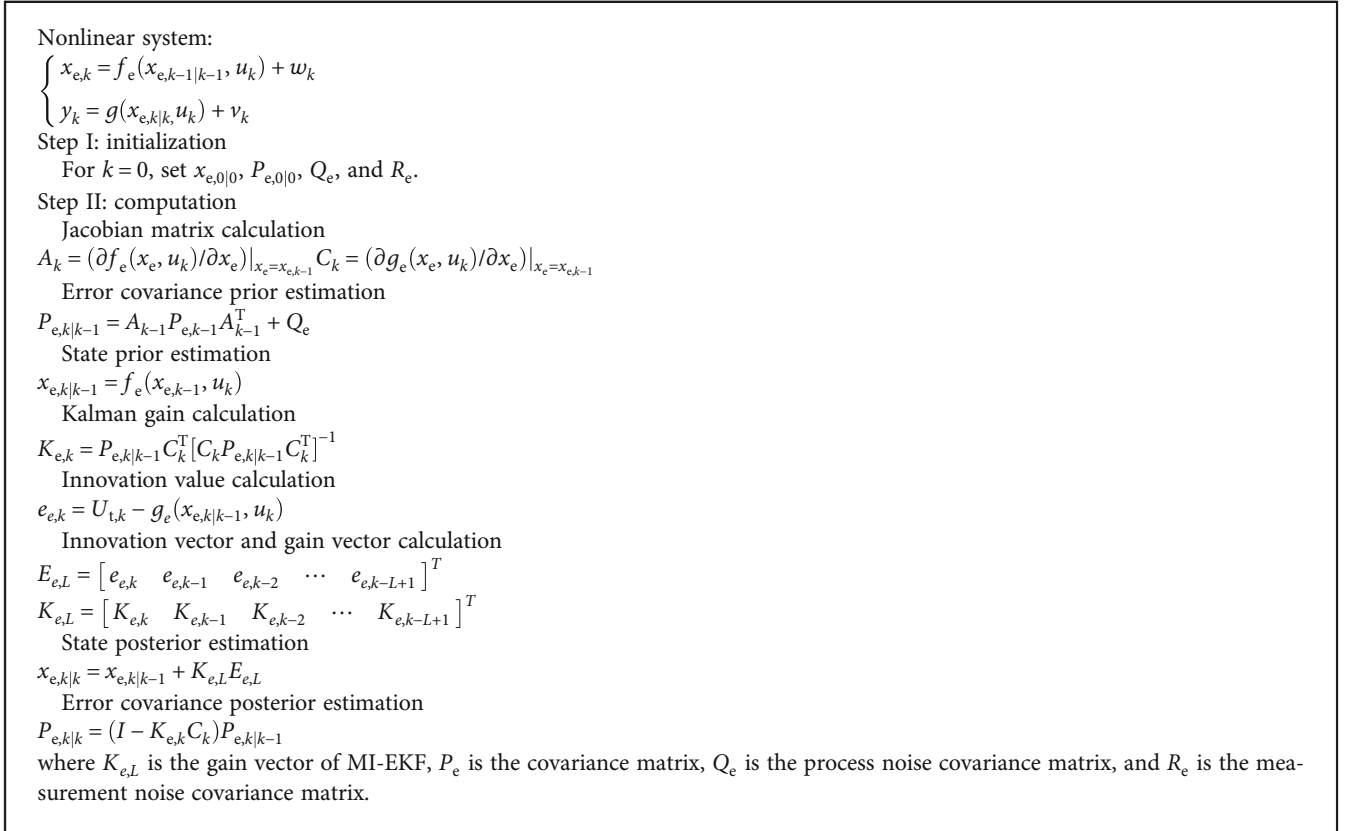capacity at present, C_{cur}, can be calculated by the AHI method by expressing the SOC as

$$SOC_t = SOC_{t_0} + \int_{t_0}^{t} \frac{\eta I_1}{C_{max}} dt, \tag{13}$$

where SOC_{t_0} and SOC_t represent the initial and current value of SOC, respectively, and η is the coulomb efficiency.

Furthermore, the discrete time form of Eq. (9) is shown as follows:

$$SOC_k = SOC_{k-1} + \frac{\eta I_{t,k}\Delta t}{C_{max}}. \tag{14}$$

Integrating Eq. (11) with representation of the polarization U_p in Eq. (2), the state space equation of LIC, that is indispensable for employing the CKF, can be obtained as follows:

Nonlinear system:
$$\begin{cases} x_{e,k} = f_e(x_{e,k-1|k-1}, u_k) + w_k \\ y_k = g(x_{e,k|k}, u_k) + v_k \end{cases}$$

Step I: initialization

For $k = 0$, set $x_{e,0|0}$, $P_{e,0|0}$, Q_e, and R_e.

Step II: computation

Jacobian matrix calculation

$$A_k = \left(\partial f_e(x_e, u_k)/\partial x_e\right)\big|_{x_e = x_{e,k-1}} \; C_k = \left(\partial g_e(x_e, u_k)/\partial x_e\right)\big|_{x_e = x_{e,k-1}}$$

Error covariance prior estimation

$$P_{e,k|k-1} = A_{k-1} P_{e,k-1} A_{k-1}^T + Q_e$$

State prior estimation

$$x_{e,k|k-1} = f_e(x_{e,k-1}, u_k)$$

Kalman gain calculation

$$K_{e,k} = P_{e,k|k-1} C_k^T \left[C_k P_{e,k|k-1} C_k^T \right]^{-1}$$

Innovation value calculation

$$e_{e,k} = U_{t,k} - g_e(x_{e,k|k-1}, u_k)$$

Innovation vector and gain vector calculation

$$E_{e,L} = \begin{bmatrix} e_{e,k} & e_{e,k-1} & e_{e,k-2} & \cdots & e_{e,k-L+1} \end{bmatrix}^T$$

$$K_{e,L} = \begin{bmatrix} K_{e,k} & K_{e,k-1} & K_{e,k-2} & \cdots & K_{e,k-L+1} \end{bmatrix}^T$$

State posterior estimation

$$x_{e,k|k} = x_{e,k|k-1} + K_{e,L} E_{e,L}$$

Error covariance posterior estimation

$$P_{e,k|k} = (I - K_{e,k} C_k) P_{e,k|k-1}$$

where $K_{e,L}$ is the gain vector of MI-EKF, P_e is the covariance matrix, Q_e is the process noise covariance matrix, and R_e is the measurement noise covariance matrix.
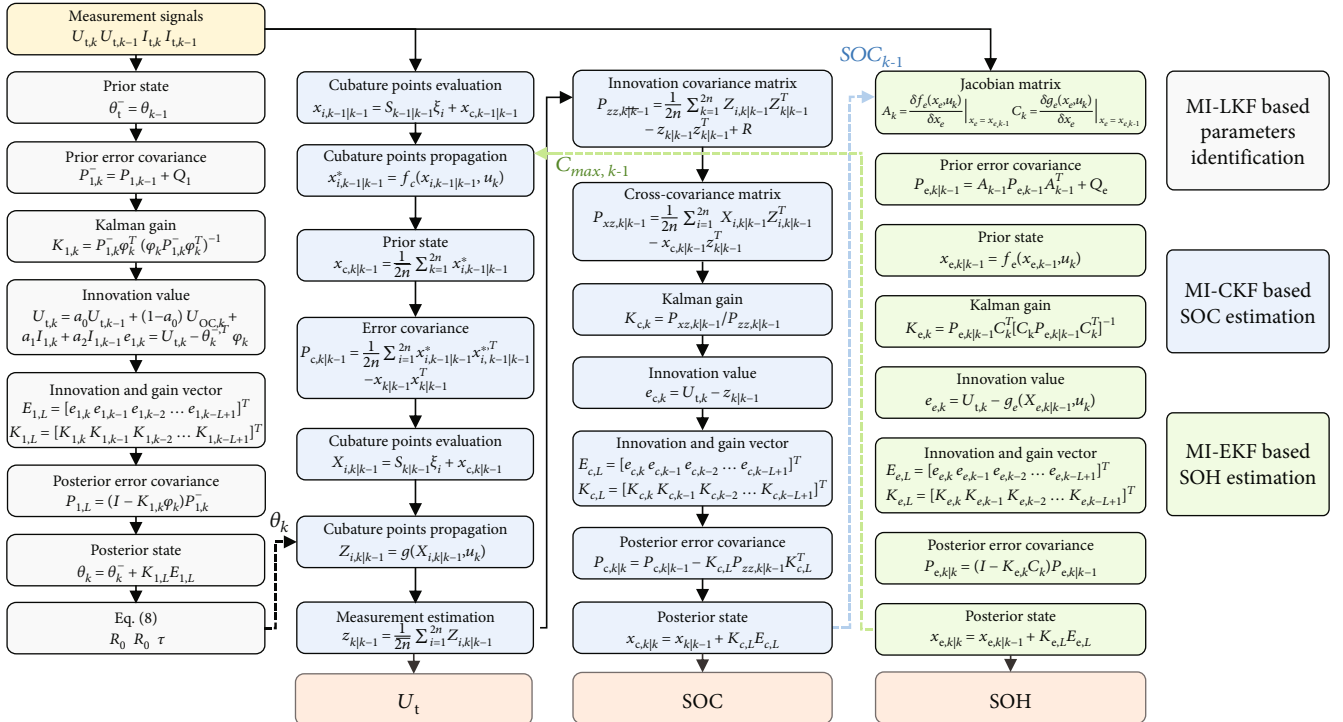
ALGORITHM 3: Recursive process of MI-EKF.

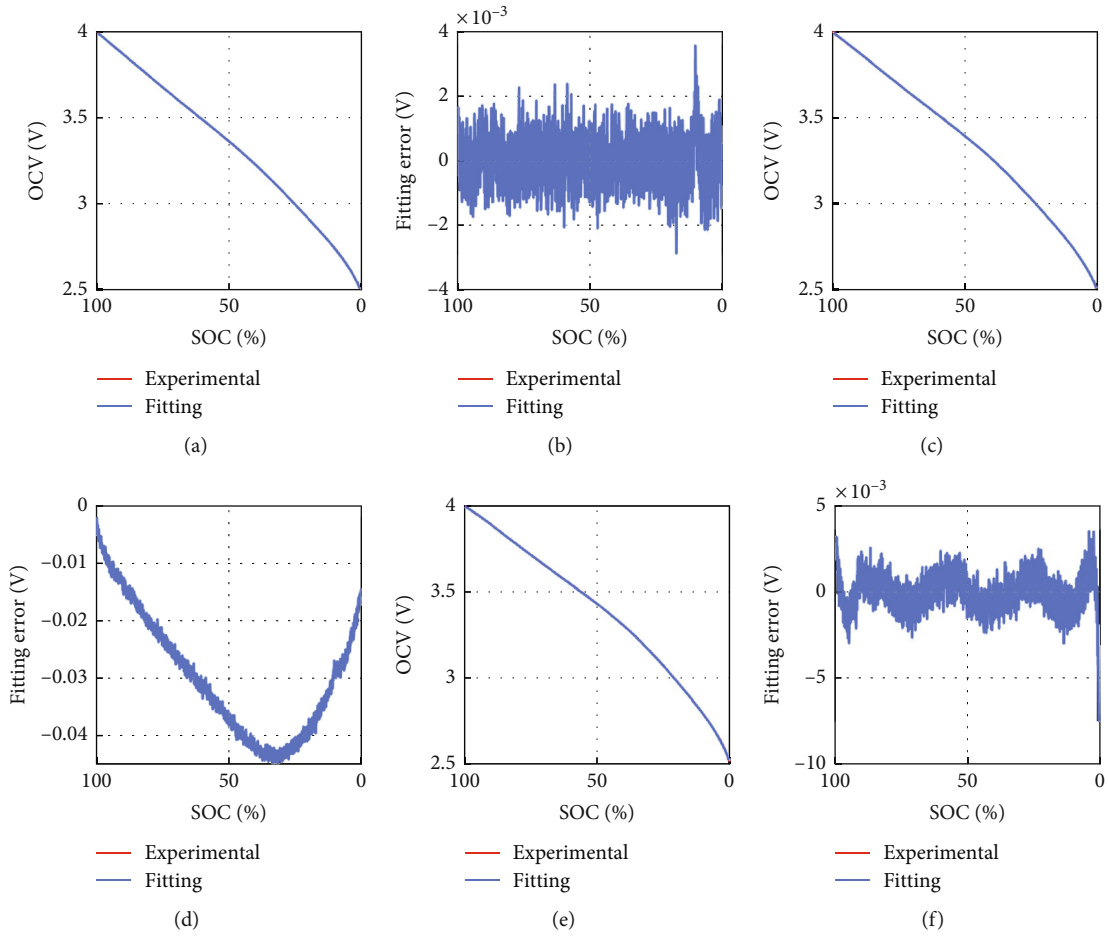FIGURE 4: Flow chart of the proposed method.

FIGURE 5: Results and corresponding OCV-SOC curve fitting: (a, b) based on discharging voltage; (c, d) based on average voltage; (e, f) based on charging voltage.
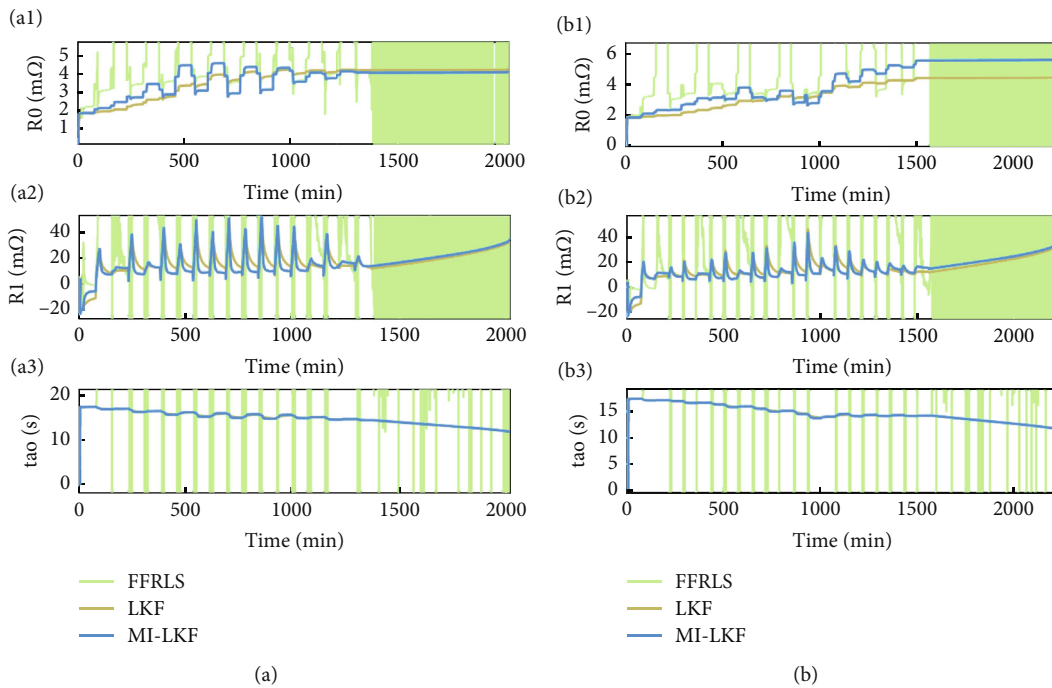

FIGURE 6: Results of parameter identification: (a1–a3) under dynamic test 1; (b1–b3) under dynamic test 2.

$$\begin{bmatrix} SOC_k \\ U_{p,k} \end{bmatrix} = \begin{bmatrix} 1 & 0 \\ 0 & \exp\left(-\dfrac{\Delta t}{R_p C_p}\right) \end{bmatrix} \begin{bmatrix} SOC_{k-1} \\ U_{p,k}-1 \end{bmatrix}$$
$$+ \begin{bmatrix} \dfrac{\eta \Delta t}{C_{max}} \\ R_0\left(1 - \exp\left(-\dfrac{\Delta t}{R_p C_p}\right)\right) \end{bmatrix} I_{l,k} + \begin{bmatrix} w_{1,k} \\ w_{2,k} \end{bmatrix},$$
$$(15)$$

where $w_{1,k}$ and $w_{2,k}$ represent the state noise.

The observation equation of LIC can be expressed as

$$U_{t,k} = U_{OC,k} + U_{p,k} + I_{l,k}R_0 + v_k, \tag{16}$$

where v_k represents the observation noise.

The CKF was proposed by Arasaratnam et al. in 2009, which is derivative-free and is regarded as an optimal approximation to the Bayesian filter that could be designed in a nonlinear system [29]. In this work, the MI-CKF is used to perform state estimation. Defining $x_c = [SOC \quad U_p]^T$ as the system state, $u = I_t$ as the system input and $z = U_t$ as the system output, the MI-CKF based SOC estimation of LIC can be processed as per the steps listed in Algorithm 2.

3.2. MI-EKF-Based SOH Estimation. The SOH is defined as the ratio of the current maximum available capacity to the nominal capacity, which is expressed as

$$SOH = \frac{C_{max}}{C_{nom}}, \tag{17}$$

where C_{max} represents the current maximum available capacity and C_{nom} is the nominal capacity.

Considering the slow varying characteristic of the capacity, the state space equation of capacity is set as

$$Q_{max,k} = Q_{max,k-1} + w_{3,k}, \tag{18}$$

where $w_{3,k}$ represents the state noise. And Eq. (11) is still used as the observation equation in SOH estimation.

From Eq. (11) and Eq. (13), we can observe that capacity and voltage are related by a very complex nonlinear relationship. Meanwhile, it is difficult to obtain a functional relationship between voltage and capacity like OCV-SOC. The EKF made local linearization to a nonlinear system by using Taylor expansion, which provides a way to decouple capacity and voltage. Hence, in this work, according to Eq. (10) and the OCV curve, first-order Taylor expansion of the observation equation based on the capacity is performed at each time step, which is expressed as

$$\frac{\partial U_t}{\partial C_{max}} = \frac{\partial U_t}{\partial SOC} \times \frac{\partial SOC}{\partial C_{max}} = \frac{\partial U_{OC}}{\partial SOC} \times \frac{\partial SOC}{\partial C_{max}}. \tag{19}$$

TABLE 1: Voltage simulation error statistics.

Test condition	Algorithm	MAE (V)	RMSE (V)
	FFRLS	0.0271	0.0443
Dynamic test 1	LKF	0.0014	0.0173
	MI-LKF	0.0013	0.0173
	FFRLS	0.0125	0.0250
Dynamic test 2	LKF	0.0019	0.0173
	MI-LKF	0.0014	0.0171

Furthermore, define $A_k = 1$ and $C_k = \partial U_{OC}/\partial SOC|_{SOC=SOC_{k-1}} \times \partial SOC/\partial C_{max}|_{C_{max}=C_{max,k-1}}$; the EKF-based SOH estimation of LIC can be conducted. It should be noted that capacity is a slowly changing parameter. In order to make the estimation more efficient and reliable, this work uses MI algorithm to improve the EKF; thus, the MI-EKF can be processed as the steps listed in Algorithm 3.

Based on the above framework, the online parameter identification and coestimation of SOC and SOH for LIC can be implemented follow the flow chart illustrated in Figure 4.

4. Experimental Analysis

In this work, a LIC with capacity of 5 Ah was tested under various conditions to validate the proposed method. The tests were carried out at room temperature under two custom dynamic tests.

4.1. OCV Curve Fitting Results. The results of OCV curve fitting and corresponding errors are shown in Figure 5. As shown in the results, the fitting errors are limited within $\pm 4 \times 10^{-3}$ V, ± 0.05 V, and $\pm 8 \times 10^{-3}$ V, respectively, which indicate that the fitting curves have high accuracy. However, the three curves show a deviation within about 40 mV between each other, which may lead to significant performance differences on the estimation of states.

4.2. Parameter Identification. The parameter identification results of MI-LKF are shown in Figure 6. With increasing time, the ohmic resistance and polarization resistance increase (i.e., SOC decreases), while the time constant decreases. Although under various test condition values of the parameters are different, overall trends are the same. It implies that under various test conditions, the proposed method has similar ability to identify parameters. The parameter accuracy is verified according to eq. (2), and the results are listed in Table 1. Along with the results depicted in Figure 6, it suggests that the model established with MI-LKF outperforms that with forgetting factor least squares (FFRLS) and LKF. Due to strong fluctuations in the parameters obtained by FFRLS, significant errors cannot be avoided. While the smaller error indicates that MI-LKF has better simulation ability for the model under dynamic conditions.
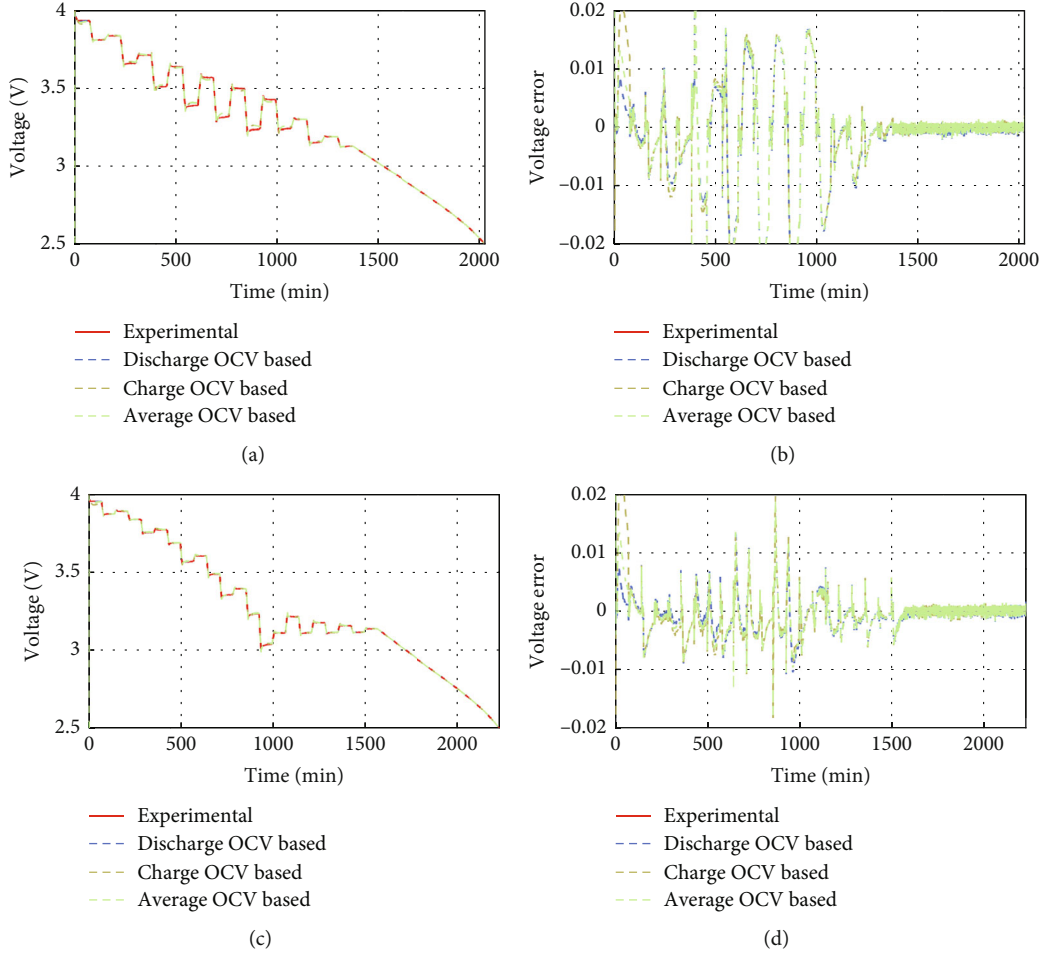
(a)

(b)

(c)

(d)

FIGURE 7: Results of voltage estimation and corresponding errors: (a, b) under dynamic test 1; (c, d) under dynamic test 2.

TABLE 2: Statistical results of voltage estimation error.

Test condition	OCV data source	MAE (V)	RMSE (V)
Dynamic test 1	Discharge OCV based	0.0010	0.0169
	Average OCV based	0.0010	0.0170
	Charge OCV based	0.0009	0.0169
Dynamic test 2	Discharge OCV based	0.0008	0.0172
	Average OCV based	0.0008	0.0172
	Charge OCV based	0.0008	0.0172

4.3. SOC Estimation. The results of voltage estimation along with the corresponding errors are shown in Figure 7, and the statistical mean absolute error (MAE) and root mean square error (RMSE) values are shown in Table 2. As illustrated in Figure 7, the voltage estimation errors obtained by using these three OCV sources are limited within a very small range, with the difference between each other being small. It indicates well matching between the established Thevenin model and the electrical behavior of LIC. Besides, based on the slight difference between the three results, it can be inferred that the discharge OCV-based one is more suitable.

The results of SOC estimation along with the corresponding errors are shown in Figure 8, while the statistical results are shown in Table 3. In this part, impact of OCV curve on the SOC estimation error becomes particularly obvious. Adopting discharge OCV limits the estimation error within ±1% (with MAE ≤ 0.51% and RMSE ≤ 0.61%). However, switching to the average OCV results in an increase of the MAE to more than 2.46% (charge OCV in 4.33%), while the RMSE also increases to more than 2.62% (charge OCV in 4.61%). It should be noted that the initial SOC is set as 100%, implying 0% initial error. This confirms
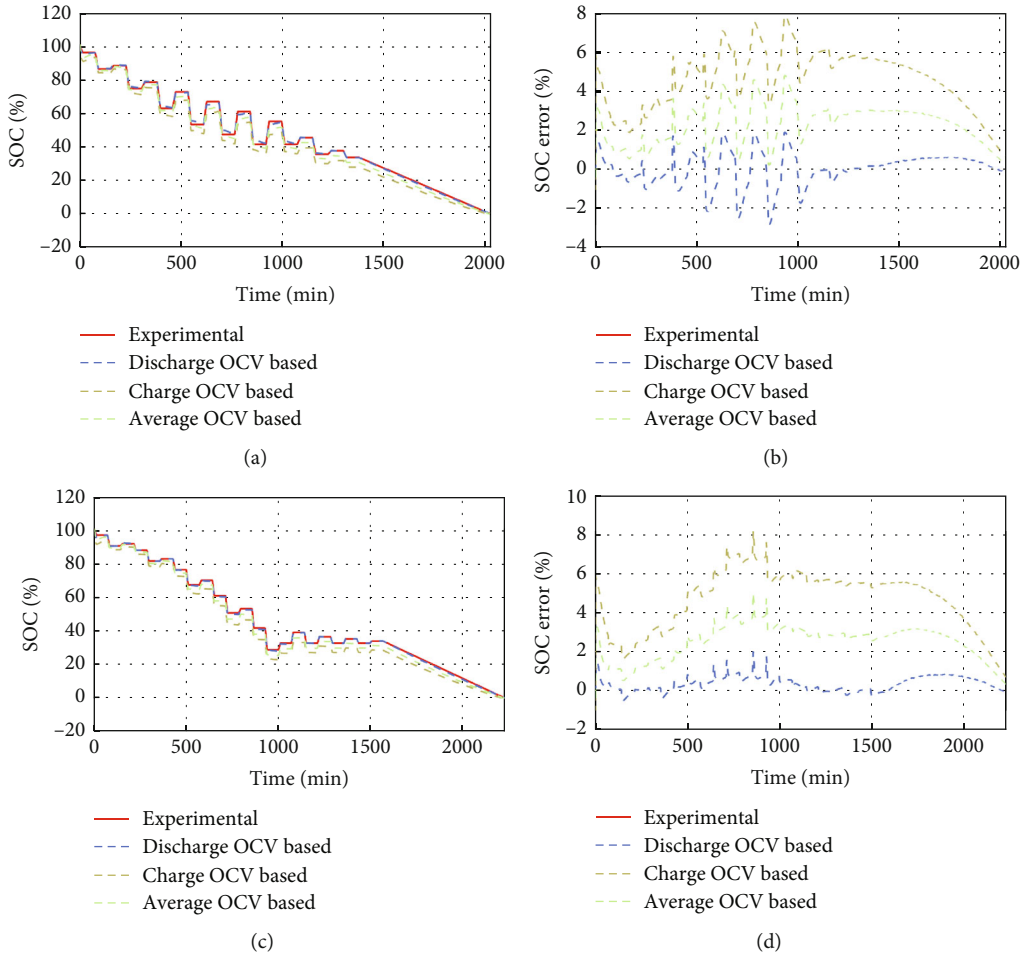
FIGURE 8: Results of SOC estimation and corresponding errors: (a, b) under dynamic test 1; (c, d) under dynamic test 2.

TABLE 3: Statistical results of the SOC estimation error.

Test condition	OCV data source	MAE (%)	RMSE (%)
	Discharge OCV based	0.47	0.57
Dynamic test 1	Average OCV based	2.36	2.51
	Charge OCV based	4.31	4.58
	Discharge OCV based	0.51	0.61
Dynamic test 2	Average OCV based	2.46	2.62
	Charge OCV based	4.33	4.61

the analysis based on voltage estimation error, and the discharge OCV is more suitable for establishing LIC model and further SOC estimation.

Figure 9 depicts the comparison results between the proposed MIF method and four commonly used algorithms for SOC estimation, including the EKF [30], the H infinity filter (HIF) [29], the CKF [31], and the square-root cubature Kalman filter (SRCKF) [32], where for such algorithms, the parameters are obtained with FFRLS. In addition, the statistical results of estimation error are listed in Table 4. It can be observed that unlike other algorithms that exhibit strong

fluctuations in SOC estimation under long-term constant current conditions, results obtained by MIF can converge to experimental value with high precision. The MAE and RMSE are limited within 0.47% and 0.55%, respectively. It is a significant improvement compared to the MAE of over 3% and RMSE of over 4% obtained by other algorithms. Furthermore, this indicates that the MIF method has greatly improved the accuracy of SOC estimation by incorporating more innovations, eliminating the need for more complex methods, which is of positive significance for the practical application of the model-based method.
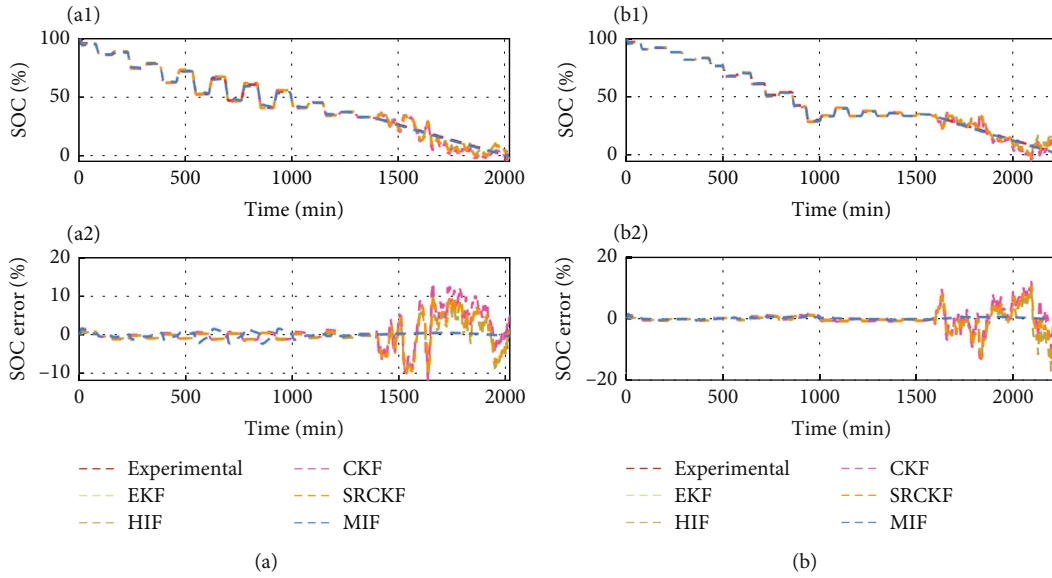
FIGURE 9: Results of voltage and SOC estimation and corresponding errors: (a1, a2) under dynamic test 1; (b1, b2) under dynamic test 2.

TABLE 4: Statistical results of the proposed method.

Conditions	Algorithms	MAE (%)	RMSE (%)
	EKF	3.96	5.36
	HIF	3.03	4.11
Dynamic test 1	CKF	3.95	5.35
	SRCKF	3.29	4.40
	MIF	0.44	0.53
	EKF	3.03	4.39
	HIF	3.19	4.60
Dynamic test 2	CKF	3.03	4.38
	SRCKF	3.09	4.35
	MIF	0.47	0.55

The initial value of the estimate algorithm plays a crucial role in SOC estimation, as it can significantly impact the accuracy of the estimation algorithm. To validate the reliability of the proposed method, experiments with four different initial values for MIF are conducted, and the corresponding results are presented in Figure 10. The figure clearly indicates that the convergence time is primarily influenced by the initial error. Specifically, as the initial value increases, the convergence time also increases. However, it is worth noting that the SOC estimation can converge to a high level of precision in less than 10 minutes. Furthermore, once the SOC estimation has converged, the estimation errors remain nearly the same regardless of the magnitude of the initial error. This observation underscores the robustness of the proposed method in handling initial SOC errors and highlights its ability to provide consistent and reliable SOC estimations.

In practical applications, LICs may not start working at full charge state, which means that the SOC corresponding to the actual initial operating point of the LIC may be unknown. In this work, the proposed method is validated at different initial operating points of LIC, where the actual initial values of SOC are 80%, 60%, and 40%, and results are illustrated in Figure 11. As it depicts, the initial value of MIF is set to 100%, which means that the maximum error from the actual initial operating point of SOC is 60%. Nevertheless, the proposed MIF can quickly track to the actual operating point of the LIC in a short period of time, with an error limit of ±3%, indicating the good robustness of the proposed method in dealing with such uncertainty.

The potential error caused by measurement noise cannot be ignored. This work validates the performance of proposed method under noise disturbance as well. Gaussian noise is added to the raw current and current data, where the intensity of current noise is 25 mA and 75 mA, and the intensity of voltage noise is 1 mV and 2.5 mV. SOC estimation results under such disturbance are depicted in Figure 12. Overall, the increase in noise intensity can lead to an increase in SOC estimation error, but MIF can still limit the error to within ±3%, indicating the robustness of the proposed method in dealing with such uncertainties.

4.4. SOH Estimation. The SOH estimation results and corresponding errors are shown in Figure 13 (a1–b2). It should be noted that for comparison, the R-based estimation results are shown in Figure 13 (c1, c2) as it associated with SOH as well [33], where the internal resistance is estimated using method reported in [34]. Results suggest that compared to the deviation from experimental values obtained by the EKF-CKF, the proposed MIF method can estimate SOH with higher accuracy (with error limited within ±0.5%). Meanwhile, the results of the R-based method showed
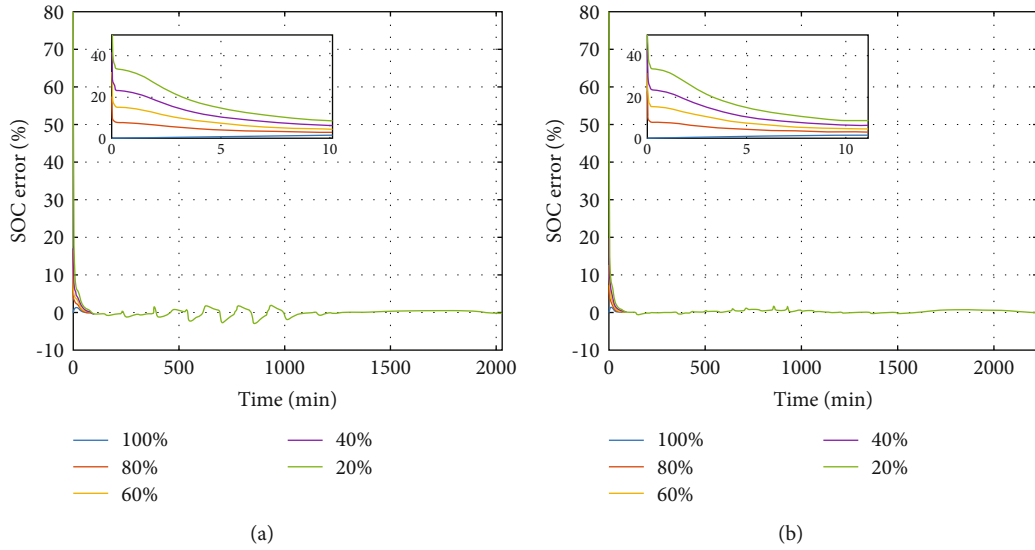
FIGURE 10: SOC estimation errors with various initial value: (a) under dynamic test 1; (b) under dynamic test 2.
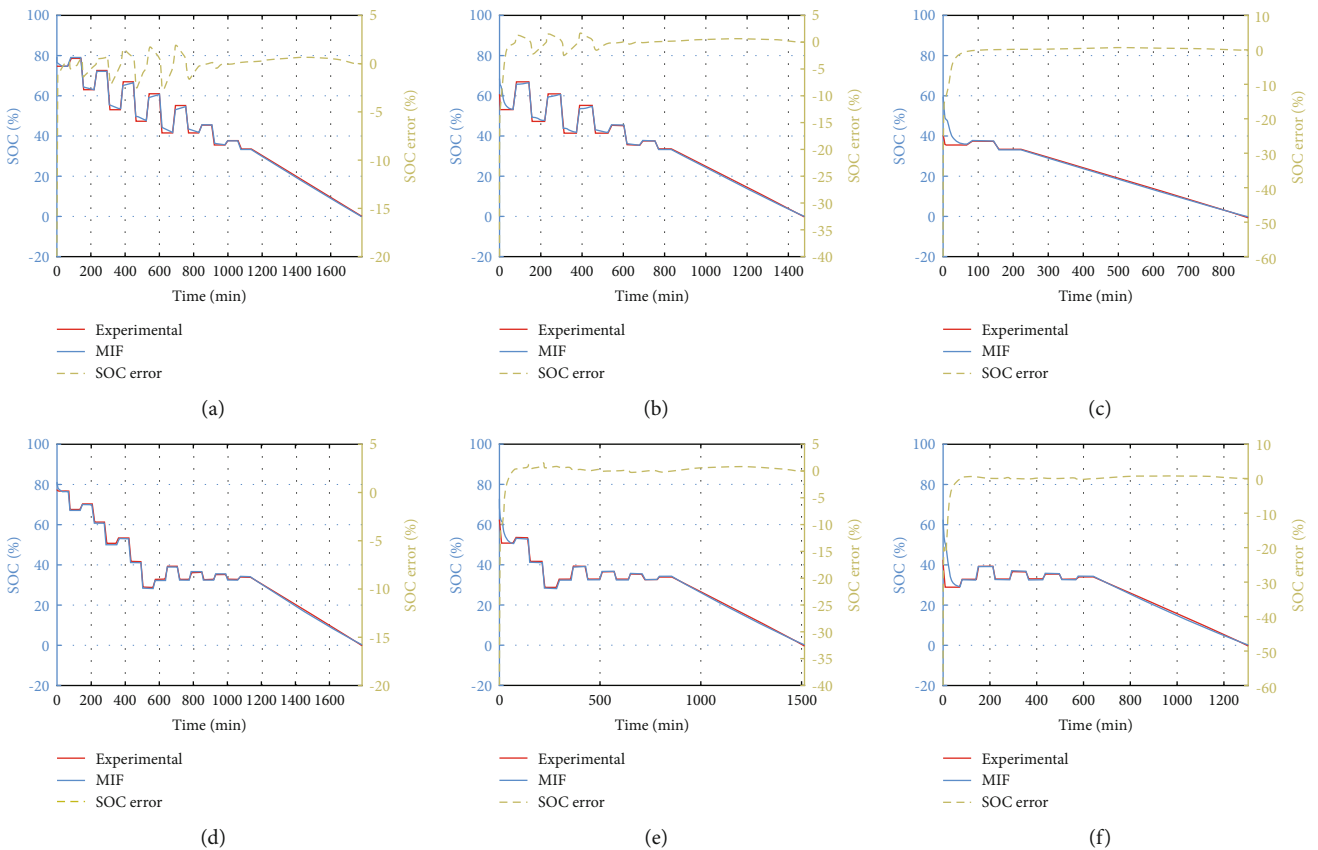

FIGURE 11: SOC estimation at various initial operating point: (a–c) under dynamic test 1; (d–f) under dynamic test 2.

significant fluctuations, especially during the low rate discharge stage at the end of the operating conditions. It indicates that the method proposed in this work has a more accurate and reliable estimation ability in such application scenarios.

Figure 14 illustrates the SOH estimation results with different initial values. It can be seen that the estimated value of MIF needs to be iteratively calculated for a certain period of time before it can track the experimental value. This may be because the capacity of the battery is a slowly changing
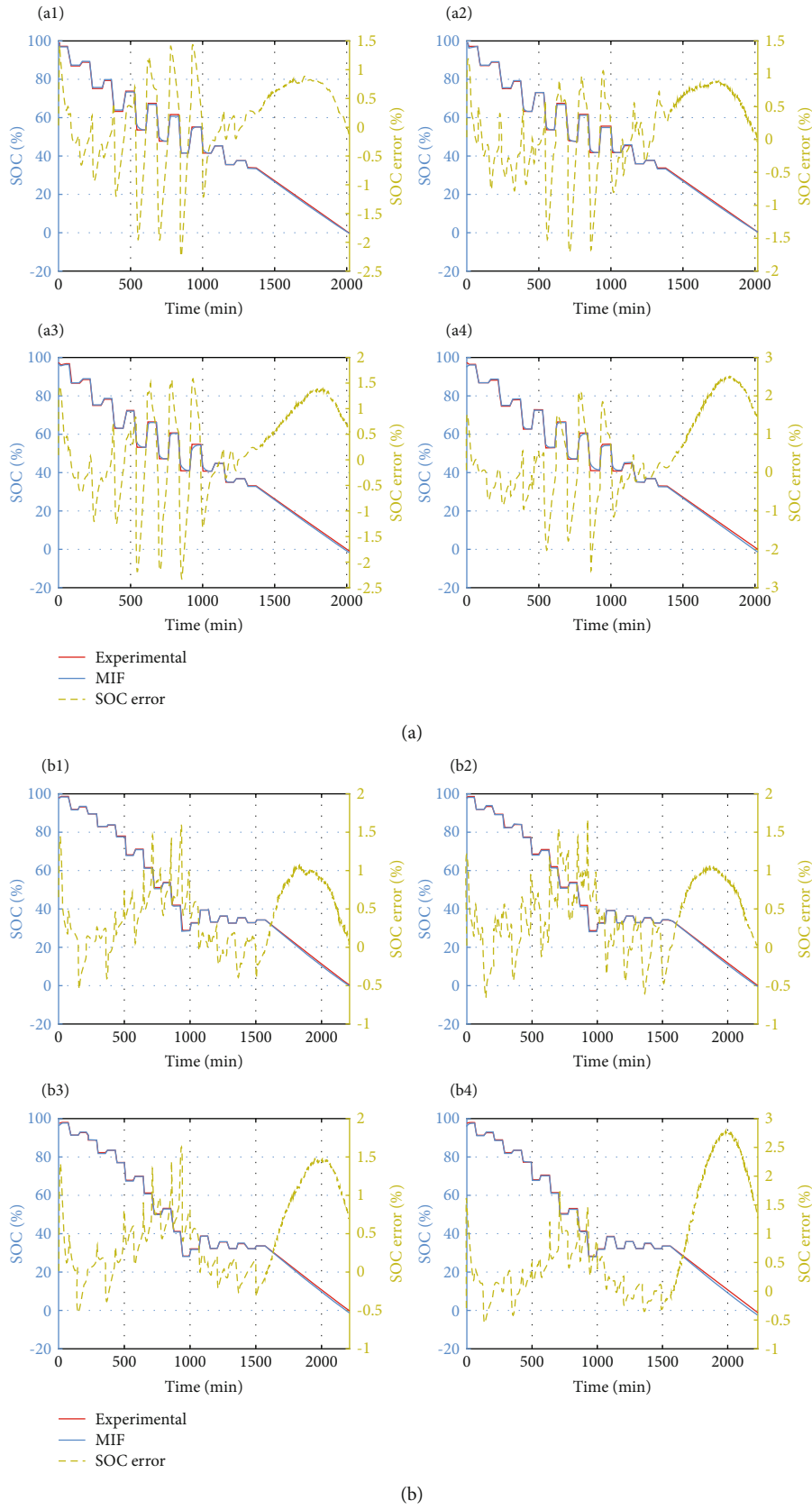
Figure 12: SOC estimation under various noise disturbance: (a1, a2) σ_I set to 25 mA and 75 mA, under dynamic test 1; (a3, a4) σ_V set to 1 mV and 2.5 mV, under dynamic test 1; (b1, b2) σ_I set to 25 mA and 75 mA, under dynamic test 2; (b3, b4) σ_V set to 1 mV and 2.5 mV, under dynamic test 2.
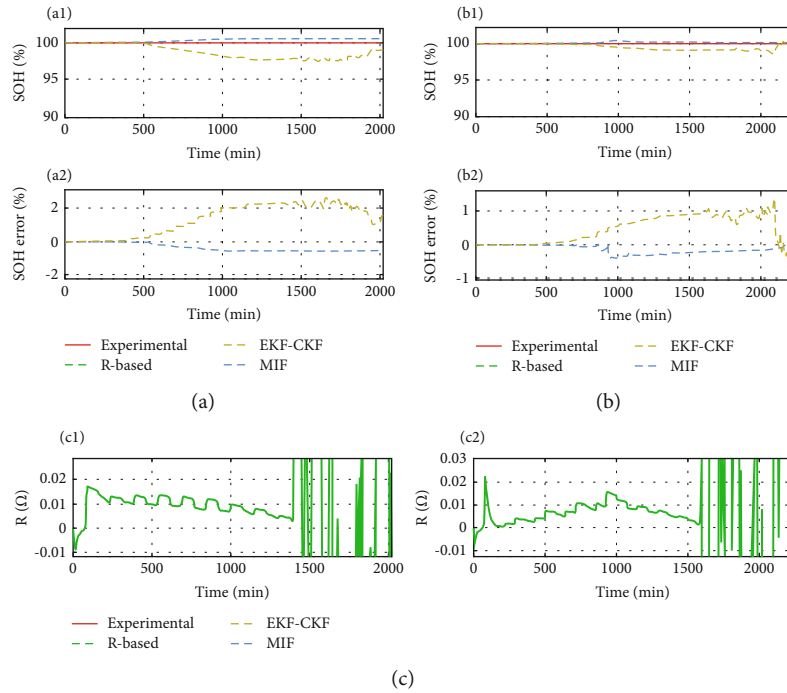
Figure 13: Results of SOH estimation and corresponding errors with initial SOH = 95%: (a1, a2) capacity-based method under dynamic test 1; (b1, b2) capacity-based method under dynamic test 2; (c1, c2) resistance-based method under dynamic tests 1 and 2.
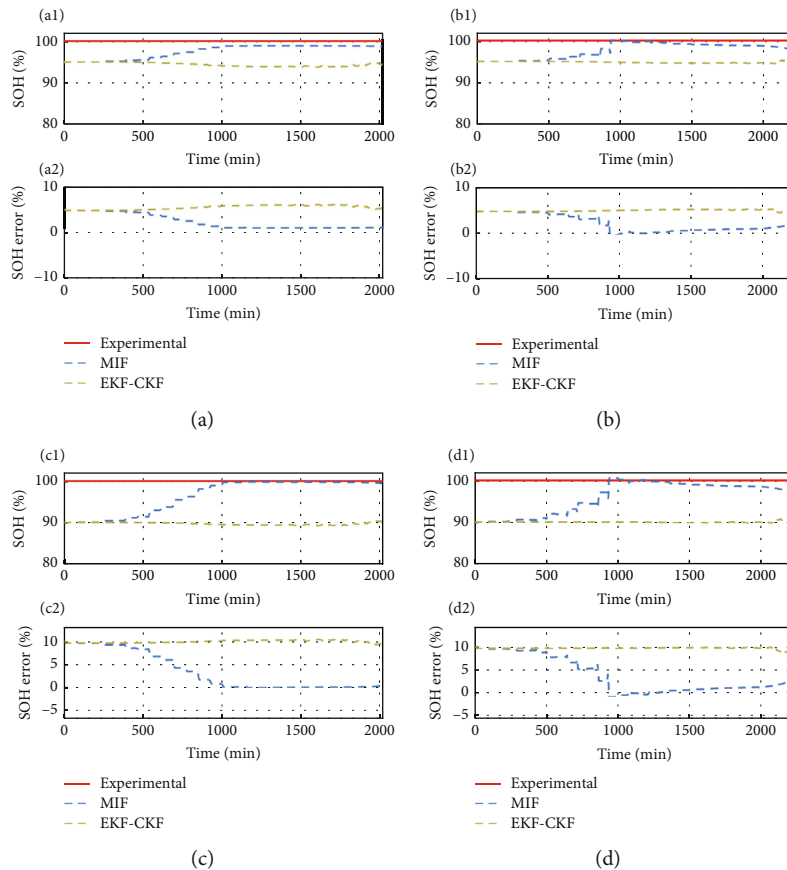

Figure 14: Results of SOH estimation and corresponding errors with initial SOH set to 95% and 90%: (a1, a2) initial SOH = 95%, under dynamic test 1; (b1, b2) initial SOH = 95%, under dynamic test 2; (c1, c2) initial SOH = 90%, under dynamic test 1; (d1, d2) initial SOH = 90%, under dynamic test 2.

parameter, and the information reflected only by the error between the battery model voltage and the actual voltage is idle. Nevertheless, even if the initial error reaches 10%, the MIF method can still limit the error to a very small range (3%), indicating that the proposed method is effective and robust in estimating the SOH of LIC.

5. Conclusion

As a new type of energy storage device, accurate modeling and reliable and efficient state estimation are the key to promote the application of LIC. In this work, a multifilter-based SOC-SOH coestimation method for LIC is proposed. The LIC is modeled by the Thevenin model, the model parameters are identified by MI-LKF, the SOC is estimated by MI-CKF, and the SOH is estimated by MI-EKF. Under various test conditions, when the initial capacity is correct, the MAE and RMSE of voltage estimation error are limited within 0.0010 V and 0.0172 V, respectively. The MAE and RMSE of SOC estimation error are limited within 0.47% and 0.55%. The estimation error of SOH can be constrained within ±0.5%. Robustness of the proposed method is verified under algorithm initial value uncertainty, state actual initial value uncertainty, and noise disturbance, and the results suggest that the SOC estimation error is limited within ±3%. Although SOH requires a certain number of iterations to converge, its error can also be constrained within 3%. In summary, MIF can achieve accurate SOC and SOH estimation of LIC and has satisfactory robustness, making it suitable for practical applications.

Data Availability

Data will be made available on request.

Conflicts of Interest

The authors declare that they have no conflicts of interest.

Authors' Contributions

Fanqi Min and Shiyi Fu contributed equally to this work.

Acknowledgments

References

[1] J. Hou, R. Zhang, P. Liu, and L. Zhou, "A review and comparative analysis on energy transition in major industrialized countries," *International Journal of Energy Research*, vol. 45, pp. 1246–1268, 2021.

[2] A. G. Olabi, C. Onumaegbu, T. Wilberforce, M. Ramadan, M. A. Abdelkareem, and A. H. al – Alami, "Critical review of energy storage systems," *Energy*, vol. 214, article 118987, 2021.

[3] E. Bullich-Massagué, F.-J. Cifuentes-García, I. Glenny-Crende et al., "A review of energy storage technologies for large scale photovoltaic power plants," *Applied Energy*, vol. 274, article 115213, 2020.

[4] H. Yang, X. Sun, Y. An, X. Zhang, T. Wei, and Y. Ma, "Online parameters identification and state of charge estimation for lithium-ion capacitor based on improved cubature Kalman filter," *Journal of Energy Storage*, vol. 24, article 100810, 2019.

[5] S. Barcellona, F. Ciccarelli, D. Iannuzzi, and L. Piegari, "Overview of lithium-ion capacitor applications based on experimental performances," *Electric Power Components and Systems*, vol. 44, no. 11, pp. 1248–1260, 2016.

[6] B. Li, J. Zheng, H. Zhang et al., "Electrode materials, electrolytes, and challenges in nonaqueous lithium-ion capacitors," *Advanced Materials*, vol. 30, no. 17, article e1705670, 2018.

[7] C. Li, X. Zhang, K. Wang, X. Sun, and Y. Ma, "A 29.3 Wh kg−1 and 6 kW kg−1 pouch-type lithium-ion capacitor based on SiOx/graphite composite anode," *Journal of Power Sources*, vol. 414, pp. 293–301, 2019.

[8] L. Zhang, X. Hu, Z. Wang, F. Sun, and D. G. Dorrell, "A review of supercapacitor modeling, estimation, and applications: a control/management perspective," *Renewable and Sustainable Energy Reviews*, vol. 81, pp. 1868–1878, 2018.

[9] J. M. Campillo-Robles, X. Artetxe, K. del Teso Sanchez et al., "General hybrid asymmetric capacitor model: validation with a commercial lithium ion capacitor," *Journal of Power Sources*, vol. 425, pp. 110–120, 2019.

[10] S. A. Hamidi, E. Manla, and A. Nasiri, "Li-ion batteries and Li-ion ultracapacitors: Characteristics, modeling and grid applications," in *2015 IEEE Energy Conversion Congress and Exposition (ECCE)*, pp. 4973–4979, Montreal, QC, Canada, 2015.

[11] N. E. Ghossein, J. P. Salameh, N. Karami, M. E. Hassan, and M. B. Najjar, "Survey on electrical modeling methods applied on different battery types," in *2015 Third International Conference on Technological Advances in Electrical, Electronics and Computer Engineering (TAEECE)*, pp. 39–44, Beirut, Lebanon, 2015.

[12] Y. Wang, G. Gao, X. Li, and Z. Chen, "A fractional-order model-based state estimation approach for lithium-ion battery and ultra-capacitor hybrid power source system considering load trajectory," *Journal of Power Sources*, vol. 449, article 227543, 2020.

[13] X. Hu, S. Li, H. Peng, and F. Sun, "Charging time and loss optimization for LiNMC and LiFePO$_4$ batteries based on equivalent circuit models," *Journal of Power Sources*, vol. 239, pp. 449–457, 2013.

[14] W. Chen, C. Xu, M. Chen, K. Jiang, and K. Wang, "A novel fusion model based online state of power estimation method for lithium-ion capacitor," *Journal of Energy Storage*, vol. 36, article 102387, 2021.

[15] X. Hu, F. Feng, K. Liu, L. Zhang, J. Xie, and B. Liu, "State estimation for advanced battery management: key challenges and future trends," *Renewable and Sustainable Energy Reviews*, vol. 114, article 109334, 2019.

[16] H. Dai, B. Jiang, X. Hu, X. Lin, X. Wei, and M. Pecht, "Advanced battery management strategies for a sustainable energy future: multilayer design concepts and research trends," *Renewable and Sustainable Energy Reviews*, vol. 138, article 110480, 2021.

[17] Z. Wei, J. Zhao, D. Ji, and K. J. Tseng, "A multi-timescale estimator for battery state of charge and capacity dual estimation

based on an online identified model," *Applied Energy*, vol. 204, pp. 1264–1274, 2017.

[18] L. Zheng, L. Zhang, J. Zhu, G. Wang, and J. Jiang, "Co-estimation of state-of-charge, capacity and resistance for lithium-ion batteries based on a high-fidelity electrochemical model," *Applied Energy*, vol. 180, pp. 424–434, 2016.

[19] M. Ragone, V. Yurkiv, A. Ramasubramanian, B. Kashir, and F. Mashayek, "Data driven estimation of electric vehicle battery state-of-charge informed by automotive simulations and multi-physics modeling," *Journal of Power Sources*, vol. 483, article 229108, 2021.

[20] Z. Shi, J. Xu, M. Wu et al., "An improved adaptive square root cubature Kalman filter method for estimating state-of-charge of lithium-ion batteries," *Journal of Energy Storage*, vol. 72, article 108245, 2023.

[21] A. Nefraoui, K. Kandoussi, M. Louzazni, A. Boutahar, R. Elotmani, and A. Daya, "Optimal battery state of charge parameter estimation and forecasting using non-linear autoregressive exogenous," *Materials Science for Energy Technologies*, vol. 6, pp. 522–532, 2023.

[22] G. L. Plett, "Extended Kalman filtering for battery management systems of LiPB-based HEV battery packs," *Journal of Power Sources*, vol. 134, no. 2, pp. 277–292, 2004.

[23] Z. Li, S. Shen, Z. Zhou, Z. Cai, W. Gu, and F. Zhang, "Novel method for modelling and adaptive estimation for SOC and SOH of lithium-ion batteries," *Journal of Energy Storage*, vol. 62, article 106927, 2023.

[24] X. Hu, S. Li, and H. Peng, "A comparative study of equivalent circuit models for Li-ion batteries," *Journal of Power Sources*, vol. 198, pp. 359–367, 2012.

[25] S. Song, X. Zhang, C. Li et al., "Equivalent circuit models and parameter identification methods for lithium-ion capacitors," *Journal of Energy Storage*, vol. 24, article 100762, 2019.

[26] S. Fu, T. Lv, W. Liu, L. Wu, C. Luo, and J. Xie, "Study of impacts of parameters identification methods on model-based state estimation for LiFePO$_4$ battery," *Ionics*, vol. 28, no. 7, pp. 3321–3339, 2022.

[27] S. Fu, W. Liu, W. Luo et al., "State of charge estimation of lithium-ion phosphate battery based on weighted multi-innovation cubature Kalman filter," *Journal of Energy Storage*, vol. 50, article 104175, 2022.

[28] F. Ding and T. Chen, "Performance analysis of multi-innovation gradient type identification methods," *Automatica*, vol. 43, no. 1, pp. 1–14, 2007.

[29] Y. Liu, S. Wang, Y. Xie, C. Fernandez, J. Qiu, and Y. Zhang, "A novel adaptive H-infinity filtering method for the accurate SOC estimation of lithium-ion batteries based on optimal forgetting factor selection," *International Journal of Circuit Theory and Applications*, vol. 50, no. 10, pp. 3372–3386, 2022.

[30] Z. Cui, W. Hu, G. Zhang, Z. Zhang, and Z. Chen, "An extended Kalman filter based SOC estimation method for Li-ion battery," *Energy Reports*, vol. 8, pp. 81–87, 2022.

[31] H. Li, H. Sun, B. Chen et al., "A cubature Kalman filter for online state-of-charge estimation of lithium-ion battery using a gas-liquid dynamic model," *Journal of Energy Storage*, vol. 53, article 105141, 2022.

[32] L. Chen, W. Yu, G. Cheng, and J. Wang, "State-of-charge estimation of lithium-ion batteries based on fractional-order modeling and adaptive square-root cubature Kalman filter," *Energy*, vol. 271, article 127007, 2023.

[33] S. B. Sarmah, P. Kalita, A. Garg et al., "A Review of State of Health Estimation of Energy Storage Systems: Challenges and Possible Solutions for Futuristic Applications of Li-Ion Battery Packs in Electric Vehicles," *Journal of Electrochemical Energy Conversion and Storage*, vol. 16, no. 4, article 040801, 2019.

[34] S. Liu, X. Dong, X. Yu, X. Ren, J. Zhang, and R. Zhu, "A method for state of charge and state of health estimation of lithium-ion battery based on adaptive unscented Kalman filter," *Energy Reports*, vol. 8, pp. 426–436, 2022.